ROBUST DYNAMIC STIFFNESS DESIGN OF A LINEAR SERVO SYSTEM

Bin-Hong Shen[1], **Mi-Ching Tsai** [1], **and Da-Wei Gu**[2]

[1]*Department of Mechanical Engineering, National Cheng Kung University, Tainan 701, Taiwan*
[2]*Department of Engineering, University of Leicester, Leicester, UK*

Abstract: As a popular controller used in the industrial servo drives, the pseudo derivative feedback with feedforward (PDFF) scheme has 3 parameters for tuning to achieve a good trade-off design between tracking and dynamic stiffness. However, the two parameters in the feedback path of the PDFF controller are restricted to constant for design simplicity that limits its dynamic stiffness. This paper presents a control design, namely "advanced PDFF controller," in that the PDFF scheme is kept, but two feedback constant gains are extended to be dynamic. An H^{∞} mixed sensitivity design is presented to systemically obtain a robust controller for dynamic stiffness design in a linear servo system. Simulation and experimental results are given to show the effectiveness of the proposed design method.

Keywords: Linear motors, H-infinity control, Servo systems, Mixed sensitivity problem, Pole assignment

1. INTRODUTION

In many feed drive control applications, linear motor possesses several features such as direct drive, high bandwidth, and high acceleration, which are very beneficial to the design of a machine tool control system. Good disturbance rejection is required as well to make a speedy restoration after load disturbance changes in linear servo systems. The property of dynamic disturbances rejection is called "dynamic stiffness". Its physical meaning is a measure of how much input force is required to cause a unit position (or velocity) deviation. Hence, a mathematical description of dynamic stiffness, k can be given by

$$k = \frac{F_d}{x} \text{ (or } \frac{F_d}{v}) \qquad (1)$$

where x and v are the position and velocity of a controlled axis and F_d is the disturbance force imposed on the axis.

Many approaches to improve the dynamic stiffness have been proposed, e.g., the state variable design methodology (Younkin and Lorenz, 1991), the inertia estimation technique (Schierling, 1988), the adaptive control (Kim and Kim, 1996), the H^{∞} control techniques (Alter and Tsao, 1996). These design methodology have their limitations when the saturation effect is considered as a tradeoff objective. A very popular scheme used in industrial servo systems is the so called pseudo derivative feedback with feedforward (PDFF) scheme (Ellis and Lorenz, 1999), as depicted in Fig.1 for the velocity loop, where all of 3 gains k_f, k_1 and k_2 are constant.

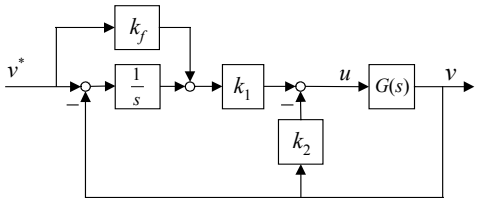

Fig. 1. The conventional PDFF control scheme.

The simplicity of the scheme in tuning parameters makes the PDFF scheme very popular. However, the conventional PDFF scheme may not yield satisfactory stability and performance when the system is subject to high order dynamic perturbations and disturbances. To result in higher dynamic stiffness and better stability robustness, the PDFF controller should be extended with dynamics. In those circumstances, an "advanced PDFF" scheme may be considered instead where k_1 and k_2 can be generalized to possibly be dynamic controllers [$K_1(s)$, $K_2(s)$].

Let $T(s) = x/F_d$ denote the transfer function from the input disturbance force to the position output. Then the minimal stiffness in frequency response function, denoted k_s, is given by

$$k_s = \left\| T(j\omega) \right\|_\infty^{-1} \tag{2}$$

Obviously, maximizing dynamic stiffness implies to minimize the H^∞-norm of $T(s)$. Therefore the maximum dynamic stiffness design problem is equivalent to a minimal H^∞-norm design problem. In this paper, the advanced PDFF control scheme is re-cast as a particular two-degree-of-freedom (2DOF) configuration where a weighted H^∞ mixed sensitivity design is proposed to achieve higher dynamic stiffness and to maintain robust stability. Moreover, by utilizing the proposed H^∞ mixed sensitivity design, there is a design freedom to maximize the dynamic stiffness via partial pole-placement, which does not increase the controller order (Tsai, *et al*., 1992). In practice, high dynamic stiffness often results in large control effort, hence a tradeoff must be considered in the mixed sensitivity design. In addition, this paper will show the pole-placement property of the proposed weighted H^∞ mixed sensitivity design by using a coprime factorization approach based on chain scattering descriptions (CSDs) and show how the advanced PDFF design is formulated into the proposed H^∞ mixed sensitivity design problem. Finally, brief design results are given to illustrate some useful properties for improving dynamic stiffness.

2. H^∞ MIXED SENSITIVITY DESIGN WITH PARTIAL POLE-PLACMENT

A coprime factorization approach based on CSDs is employed to solve the solution of the H^∞ mixed sensitivity problem in this paper for its simplicity and straight-forward property (Tsai, and Tsai, 1993). Using this approach, the general H^∞ suboptimal control problem can be formulated into two associated coupling chain scattering matrices, and the solutions can be found by solving two pairs of J-lossless coprime factorizations. The following lemma (Tsai, and Tsai, 1993) is very useful when using CSDs in H^∞ suboptimal control problem.

Lemma: Let a right CSD system G be J-lossless, then $\left\| CSD_r(G,\Phi) \right\|_\infty < 1$; if and only if (iff) $\|\Phi\|_\infty < 1$.

Dually, let a left CSD system $\tilde{G}$ be dual J-lossless, then $\left\| CSD_l(\tilde{G},\Phi) \right\|_\infty < 1$; iff $\|\Phi\|_\infty < 1$.

2.1 Pole Placement Property of the Mixed Sensitivity Design

This section will show how the pole placement can be achieved via an appropriate selection of W_d. Recall the weighted-mixed sensitivity design problem as show in Fig. 2. Let w=v_d and $z = [e_1, e_2]^T$, the closed-loop system from w to z is given by

$$LFT(P,K) = P_{11} + P_{12}(I - P_{22}K)^{-1}P_{21}. \tag{3}$$

where

$$P = \left[\begin{array}{c|c} W_1W_d & W_1G_a \\ \hline 0 & W_2 \\ \hline W_d & G_a \end{array}\right] = \left[\begin{array}{c|c} P_{11} & P_{12} \\ \hline P_{21} & P_{22} \end{array}\right]. \tag{4}$$

Consider the problem of finding a K such that

$$\left\| LFT(P(s),K(s)) \right\|_\infty < 1 \tag{5}$$

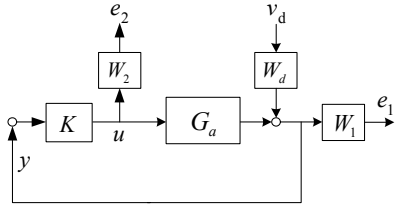

Fig. 2. Mixed sensitivity design problem

Note that we have normalized the required norm bound (γ) as 1, since it can be absorbed in W_1 and W_2. Here, W_1 and W_2 can be constant matrices to provide a simple trade-off between performance and control effort. The input weight W_d is chosen as the inverse of a left coprime denominator of the controlled plant. Let $G_a = \tilde{M}^{-1}\tilde{N}$ be a left coprime factorization (lcf) and $G_a(s) \overset{s}{=} \left[\begin{array}{c|c} A & B \\ \hline C & 0 \end{array}\right]$ be a minimal realization. Then we have

$$\left[\tilde{N}(s) \quad \tilde{M}(s)\right] \overset{s}{=} \left[\begin{array}{c|cc} A+HC & B & H \\ \hline \tilde{W}C & 0 & \tilde{W} \end{array}\right]. \tag{6}$$

where H is any gain matrix such that $A+HC$ is stable, and $\tilde{W}$ is a nonsingular constant matrix. Furthermore, the input weight W_d is selected as

$$W_d(s) = \tilde{M}^{-1}(s) \overset{s}{=} \left[\begin{array}{c|c} A & -H\tilde{W}^{-1} \\ \hline C & \tilde{W}^{-1} \end{array}\right]. \tag{7}$$

So that the poles of W_d are the same as the poles of the controlled plant G_a, and the zeros of W_d would be the eigenvalues of $A+HC$. Then the state-space realization of the Standard Control Configuration (SCC) plant P as shown in Fig. 3 can be found as

$$P(s)\overset{s}{=}\left[\begin{array}{c|c|c} A & -H\tilde{W}^{-1} & B \\ \hline \begin{pmatrix} W_1 C \\ 0 \end{pmatrix} & \begin{pmatrix} W_1\tilde{W}^{-1} \\ 0 \end{pmatrix} & \begin{pmatrix} 0 \\ W_2 \end{pmatrix} \\ \hline C & \tilde{W}^{-1} & 0 \end{array}\right]. \quad (8)$$

Note that $P_{21}(s)=\tilde{M}^{-1}(s)$ is square and its inverse is stable. The following theorem (Tsai, *et al*., 1992) shows the pole assignment properties of this specific H^∞ mixed-sensitivity design problem, and the proof of the theorem is outlined in the following section.

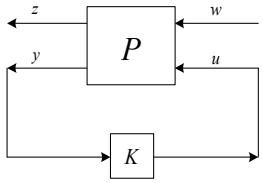

Fig. 3. A SCC of the control problem

Theorem: Let K be a solution of problem (5). Then, the eigenvalues of $A+HC$ are included in the closed-loop poles.

2.2 CSD Solutions

Following the coprime factorization approach proposed by Tsai, *et al* (1993), the LFT framework as shown in Fig. 3 can be transformed to a CSD framework in terms of two coupled CSDs as shown in Fig. 4.

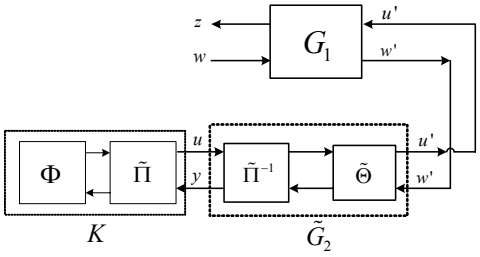

Fig. 4. Overall closed-loop system in terms of two coupling CSDs

Hence, the closed-loop system from w to z is given by

$$\begin{aligned} LFT(P,K) &= CSD_r(G_1, CSD_l(\tilde{\Pi}^{-1}\tilde{\Theta}, CSD_l(\tilde{\Pi},\Phi))) \\ &= CSD_r(G_1, CSD_l(\tilde{\Theta},\Phi)) \end{aligned} \quad (9)$$

where G_1, $\tilde{G}_2$, $\tilde{\Theta}$, and $\tilde{\Pi}$ are in $\Re H^\infty$ ($\Re H^\infty$ denotes the real rational subspace of H^∞). By appropriately choosing several constant matrices, via solving algebraic Riccati equations, G_1 and $\tilde{\Theta}$ can be made J-lossless and dual J-lossless respectively. Applying the above lemma it yields that

$$\begin{aligned} \left\|LFT(P,K)\right\|_\infty = \left\|CSD_r(G_1, CSD_l(\tilde{\Theta},\Phi))\right\|_\infty < 1 \\ \text{iff } \|\Phi\|_\infty < 1 \end{aligned} \quad (10)$$

Then the suboptimal solutions is given by

$$K = CSD_l(\tilde{\Pi},\Phi) \qquad \forall \Phi \in BH^\infty \quad (11)$$

where

$$\tilde{\Pi}(s)\overset{s}{=}\left[\begin{array}{c|cc} A+HC & -B & H \\ W_{x2}^{-1}F_{x2} & W_{x2}^{-1} & 0 \\ W_{x1}^{-1}(\tilde{W}C-F_{x1}) & 0 & W_{x1}^{-1}\tilde{W} \end{array}\right]. \quad (12)$$

In the proposed design problem, for given H and $\tilde{W}$, the suboptimal solution is to choose F_{x1}, F_{x2}, W_{x1} and W_{x2} such that G_1 is J-lossless. Note that the obtained $\tilde{\Theta}$ in this problem is an identity matrix which is dual J-lossless naturally. If Φ=0, the central controller K_0 can be obtained as

$$\begin{aligned} K_0 &= CSD_l\left(\tilde{\Pi},0\right) = -\tilde{\Pi}_{11}^{-1}\tilde{\Pi}_{12} \\ &= \left[\begin{array}{c|c} A+HC+BF_{x2} & -H \\ \hline F_{x2} & 0 \end{array}\right]. \end{aligned} \quad (13)$$

Then, it can be worked out that

$$\left(I-G_a K_0\right)^{-1} = \left[\begin{array}{cc|c} A+BF_{x2} & -HC & H \\ 0 & A+HC & -H \\ \hline C & C & I \end{array}\right]. \quad (14)$$

This shows that the eigenvalues of $A+HC$ and $A+BF_{x2}$ are the closed-loop poles resulting from the central solution.

As mentioned earlier, the suggested input weight W_d can provide an alternative for partial pole placement. Furthermore, such a selection of input weight W_d does not increase the dimension of the design problem. Although the pole placement is not a primary objective in the mixed sensitivity design, such choice of weights to achieve dynamic stiffness is very attempting.

3. H^∞ Mixed Sensitivity Design in Advanced PDFF Control for a Linear Servo System

This section shows how the advanced PDFF design is formulated into the proposed H^∞ mixed sensitivity design problem. Assume that the model of current-loop servo drive and the linear motor for speed loop controller design is represented as

$$G_m(s) = \frac{K_t}{ms+c}\overset{s}{=}\left[\begin{array}{c|c} -\frac{c}{m} & \frac{K_t}{m} \\ \hline 1 & 0 \end{array}\right] = \left[\begin{array}{c|c} A_m & B_m \\ \hline C_m & 0 \end{array}\right]. \quad (15)$$

where K_t is the force constant, m the mass and c the viscous damping coefficient of the motor. Fig. 5 shows the overall servo system where the advanced PDFF controller is implemented in the speed loop. To retain the PDFF structure, consider a pseudo

single-input-two-output plant (i.e., one force input and two outputs, position and speed) given by

$$G_a = \begin{bmatrix} -\frac{1}{s}G_m \\ G_m \end{bmatrix} \overset{s}{=} \left[\begin{array}{cc|c} -\frac{c}{m} & 0 & \frac{K_t}{m} \\ -1 & 0 & 0 \\ \hline 0 & 1 & 0 \\ 1 & 0 & 0 \end{array}\right] = \left[\begin{array}{c|c} A & B \\ \hline C & 0 \end{array}\right]. \quad (16)$$

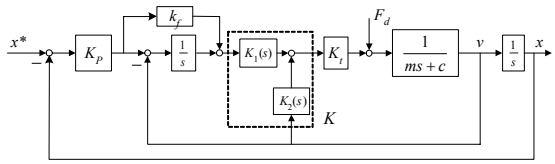

Fig. 5. The advanced PDFF scheme in cascaded-loop structure.

In the H^∞ mixed sensitivity design of speed control loop, two weighting matrices are used on the output of G_a and on the control signal, i.e. $W_1 = \begin{bmatrix} w_{1a} & 0 \\ 0 & w_{1b} \end{bmatrix}$, and $W_2 = w_2$, respectively. The input weight w_d is chosen to be the inverse of a left coprime denominator of G_m. The feedback configuration of the design problem is depicted in Fig. 6.

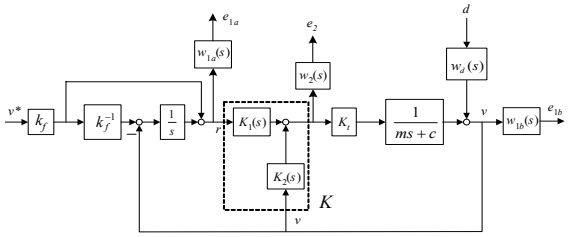

Fig. 6. Feedback configuration of the advanced PDFF control design

Now the design problem of Fig.6 is to find a stabilizing controller K= [$K_1(s)$, $K_2(s)$] such that K minimizes the H^∞-norm of the weighted closed-loop transfer function from $[v^*, d]^T$ to $[e_1, e_2]^T$ as the following, where $e_1 = [e_{1a}, e_{1b}]^T$ and $S=(I - G_aK)^{-1}$

$$\min_{K \in RH^\infty} \left\| \begin{bmatrix} W_1 S \\ W_2 KS \end{bmatrix} W_d \right\|_\infty . \quad (17)$$

The lcf of G_a can be obtained from (6) by letting $H = \begin{bmatrix} 0 & -H_m \\ k_f^{-1} & 1 \end{bmatrix}$ and $\tilde{W} = \begin{bmatrix} k_f^{-1} & 0 \\ 0 & \tilde{w} \end{bmatrix}$. From (7), choosing $W_d = \tilde{M}^{-1}$ will yield

$$W_d(s) = \begin{bmatrix} \frac{1}{s} + k_f & \frac{-1}{s} w_d \\ 0 & w_d \end{bmatrix} \overset{s}{=} \left[\begin{array}{cc|cc} -\frac{c}{m} & 0 & 0 & -H_m \tilde{w}^{-1} \\ -1 & 0 & 1 & -\tilde{w}^{-1} \\ \hline 0 & 1 & k_f & 0 \\ 1 & 0 & 0 & \tilde{w}^{-1} \end{array}\right]. \quad (18)$$

and

$$A + HC = \begin{bmatrix} -\frac{c}{m} - H_m & 0 \\ 0 & -k_f^{-1} \end{bmatrix}. \quad (19)$$

Therefore, the state-space realization of the design problem can be obtained as following figure.

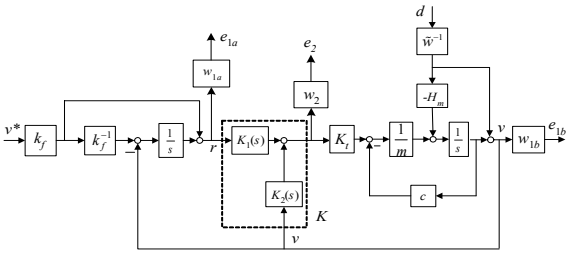

Fig. 7. State space realization of the problem

After picking up W_1, W_2, k_f, H_m and $\tilde{w}$, the controller K= [$K_1(s)$, $K_2(s)$] can be solved with the state-space realization of the generalized plant P of the problem (17). According to the Theorem in Section 2.1, the closed-loop poles resulting from the H^∞ design problem will include $\alpha = -\left(\frac{c}{m} + H_m\right)$ and $-k_f^{-1}$.

4. DESIGN EXAMPLE

A linear servomotor as shown in Fig.8 is utilized as a controlled plant in the design. The transfer function of the linear servomotor from force input to velocity output is obtained by dynamic signal analyzer (DSA) and specifications are given in Table 1. The desired position bandwidth is 25 Hz and the velocity bandwidth 100 Hz.

Table 1 Spec's of controlled plant (YOKOGAWA linear motor LM-110):

Item	value
Plant model obtained by DSA	$\frac{908.94}{s+73.59}\frac{mm/s}{N}$
Force command factor (equivalent K_t)	100 N / 8 volt
Rated force	50 N
Rated speed	0.42 m/s

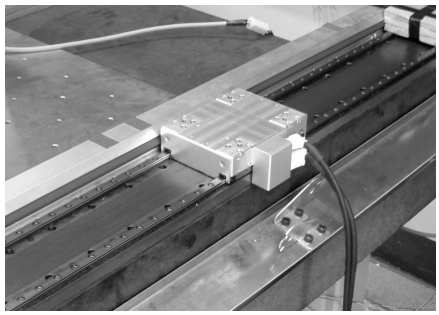

Fig. 8. Experimental setup of the linear servomotor

4.1 Proposed Advanced PDFF Design.

Without loss of generality, let $W_2(= w_2)$ be 1, then there are four parameters to be decided: w_{1a}, w_{1b}, k_f and H_m. Obviously, W_1 should be as large as possible for the sake of finite control energy. Moreover, since r, the first output signal of G_a, is the integral of the second output v, weighting on r is relative to weighting on v. Hence the weight, w_{1b} can be set to zero for the convenience of design. A design procedure for the proposed advanced PDFF controller is suggested as follows. (i). Given a desired position bandwidth, which provides a constraint in the velocity bandwidth, says 3~5 times the position bandwidth. (ii). Choose a state feedback gain H to obtain the left coprime factorization of G_a such that the initial α value (see Section 3) is slightly higher than the position bandwidth. (iii). Choose weighting gain W_1 value, and solve the controller for Problem (17). Then, evaluate the velocity loop bandwidth, and re-tuning the W_1 value until velocity loop provide with a satisfactory bandwidth (in this case, W_1 is chosen as 40). (iv). Shift α to a higher frequency to get a higher dynamic stiffness but not yet to cause an insufficient velocity bandwidth.

Table 2 and Fig. 9 show the design results for the varying α (from 30 to 180 Hz). Note that as expected by above-mentioned theorem, all the eigenvalues of $A+HC$ (α and k_f^{-1}) are the closed-loop poles but have no effects on v/v^* due to the pole-zero cancellations, however, α will influence the transfer function, x/F_d. It indicates a very important and useful property in the proposed dynamic stiffness design method: the bandwidth and the dynamic stiffness can be designed respectively by varying the weighting gains and α. The extremely high frequency mode of controller has been removed by model reduction in Table 2. It can be observed that when α is getting bigger in magnitude, the DC gain of the controller and stiffness increases, but the velocity bandwidth decreases slightly. This phenomenon can be explained by Fig.10. Fig. 10 shows the effect of shifting α more right of the dynamic stiffness plot by using the asymptotic curve. Because the dynamic stiffness is the inverse of x/F_d, it has one pole (at origin) and three zeros (containing α). In Fig. 10, the line of slope 2 is the effect of passive inertia term, the line of slope 1 is the effect of active damping, the horizontal line means static stiffness, and the line of slope -1 is the integral stiffness caused by the inherent zero at origin (Younkin and Lorenz, 1991). It can be found that α is the intersection frequency between the active damping and inertia line, hence, when α is shifted to a higher frequency, the damping line will be vertically pulled up to a higher level, and the low frequency stiffness will also be pulled up a little consequently. This implies the total dynamic stiffness come to a higher scope. Certainly, there is a limitation on increasing the α value since the velocity bandwidth should not be descended to an undesired range. Through the design procedure, a satisfactory results is obtained when choosing $\alpha = -1130.97$.

Table 2 Design results for w_{1a}= 40 and varying α

	α=-188.5 (rad/s)	α=-502.7 (rad/s)	α=-1130.9 (rad/s)
poles of v/v^*	-639.11 ***-188.50*** ***-10***	-631.23 ***-502.65*** ***-10***	-603.43 ***-1130.97*** ***-10***
zeros of v/v^*	***-188.50*** ***-10***	***-502.65*** ***-10***	***-1130.97*** ***-10***
poles of x/F_d (the inverse of dynamic stiffness)	-278.31 -360.72 ***-188.50*** ***-10***	-300.40 -330.07 ***-502.65*** ***-10***	-301 ± 63i ***-1130.97*** ***-10***
zeros of x/F_d	***-10*** 0	***-10*** 0	***-10*** 0
DC gain of K_1	132.46	346.27	742.60
DC gain of K_2	-13.37	-35.10	-75.41
Minimal stiffness	212.81 (N/mm)	396.55 (N/mm)	767.24 (N/mm)
Velocity loop bandwidth	101 (Hz)	99.7 (Hz)	95 (Hz)

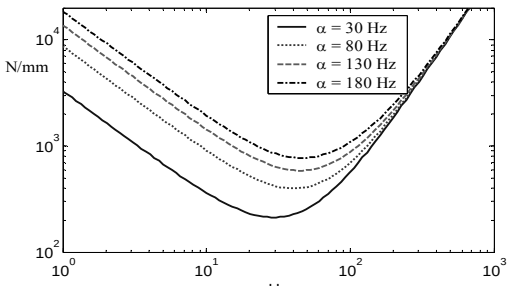

Fig. 9. Dynamic stiffness plot (F_d / x) for different α

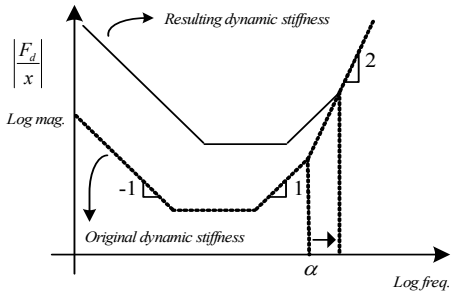

Fig. 10. The effect of shifting α in asymptotic curve

4.2 Comparison with Conventional PDFF

Comparisons between conventional PDFF control and advanced PDFF control are given in Fig.11 ~ 14. Figure 11 shows the simulated dynamic stiffness plot of the proposed advanced PDFF controller and the conventional PDFF method, it can be found that the dynamic stiffness of proposed design is higher than the conventional one. And the robustness of proposed design can be observed from the simulated and experimental step response as shown in Fig. 12 and 13. As shown in these figures, it can be seen that the proposed design provides good response under the inertial load variation, and the conventional PDFF design is sensitive to the inertial due to insufficient of dynamic stiffness on the other hand.

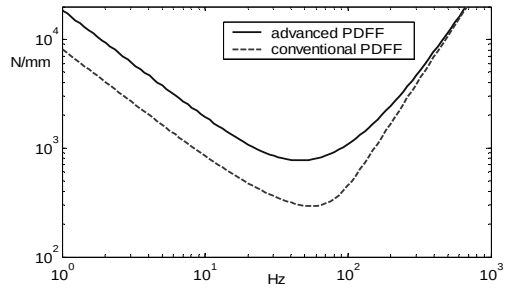

Fig. 11. The dynamic stiffness of two controllers

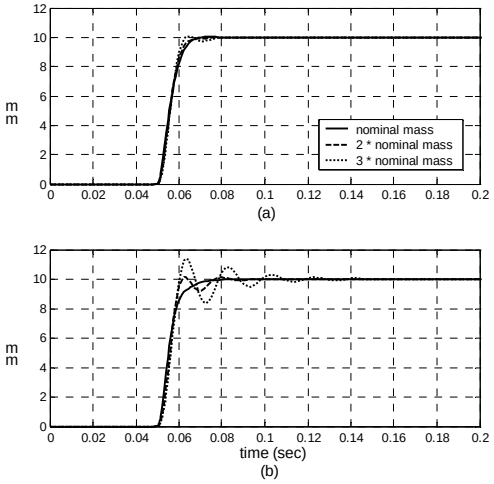

Fig. 12. Simulation results of step response under inertial load variation (a) advanced PDFF (b) PDFF controller

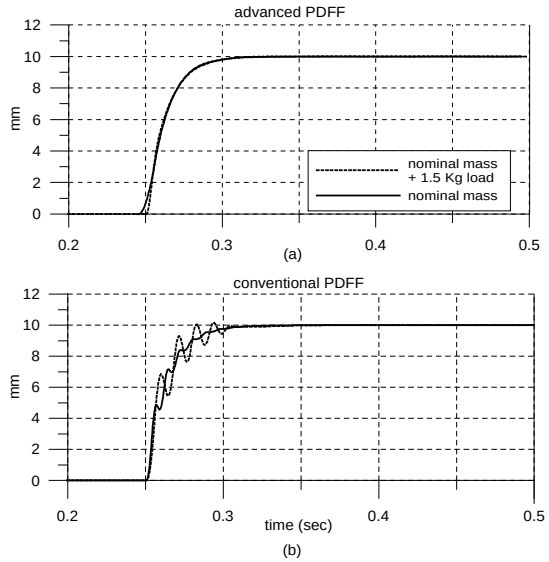

Fig. 13. Experimental results of the step response under inertial load variation (a) advanced PDFF (b) PDFF controller

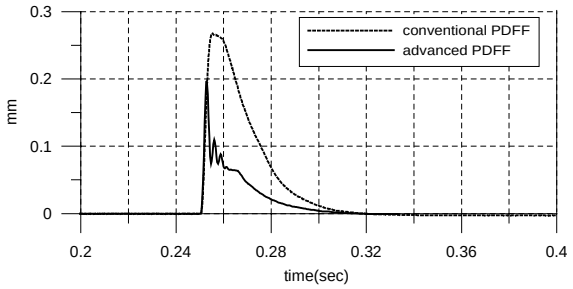

Fig. 14. Experimental results of disturbance step response (F_d = 37.5 N)

Finally, Fig. 14 shows the ability of disturbance rejection of two controllers. The maximal value of the disturbance step response is about 0.26 mm and 0.2 mm respectively, it shows that the proposed design makes a faster restoration and a smaller position deviation after load disturbance change.

5. CONCLUSION

This paper has extended the PDFF control scheme to include dynamic controllers for achieving high dynamic stiffness designs. A systematic method is proposed using H^{∞} mixed sensitivity approach on an augmented pseudo plant. A partial pole-placement technique is employed in the advanced PDFF control design to improve both dynamic stiffness and robust stability. The proposed method has been successfully applied to a linear motor system where the desired stiffness and performance are achieved by tuning the weighting gains. Design results showed that the proposed method has a special property to improve dynamic stiffness by assigning the eigenvalue of *A+HC* such that the bandwidth and dynamic stiffness can be designed sequentially under the limitation of finite control effort. Experiment and simulation results demonstrate the effectiveness and feasibility of the proposed control scheme.

REFERENCES

Alter D. M., and T. C. Tsao (1996), Control of linear motors for machine tool feed drives: design and implementation of H^{∞} optimal feedback control," *ASME J. of Dynamic Systems, Measurement, and Control*, **Vol. 118**, pp.649-656.

Ellis G. and R.D. Lorenz (1999), Comparison of motion control loops for industrial applications**,** *Proc. IEEE IAS Annual Meeting*, **Vol. 4**, pp. 2599-2605.

Gross, H. (1983). *Electrical Feed Drives for Machine Tools*, pp. 47, John Wiley & Sons, New York.

Kim T. Y., and J. Kim (1996), Adaptive cutting force control for a machining center by using indirect cutting force measurements, *Int. J. Machine Tools & Manufacture*, **Vol. 36**, pp.925-937.

Schierling H. (1988), Fast and reliable commissioning of AC variable speed drives by self-commissioning, *Proc. of IEEE IAS Annual Meeting*, pp.489-492

Tsai, M.C., E. J. M. Geddes, and I. Postlethwaite (1992). Pole-zero cancellations and closed-loop properties of an H^{∞} mixed sensitivity design problem. *Automatica,* **Vol. 34,** pp. 519-530.

Tsai, M.C. and C. S. Tsai (1993). A Chain scattering-matrix description approach to H^{∞} control. *IEEE Trans. AC,* **Vol. 38,** pp. 1416-1421.

Younkin G.W., W.D. McGlasson, R.D. Lorenz, (1991). Considerations for low-inertia AC drives in machine tool axis servo. *IEEE Transactions on Industry Applications*, **Vol. 27,** pp. 262-267.